JMEPEG (2015) 24:175–184
DOI: 10.1007/s11665-014-1300-5

1059-9495/$19.00

Blasting and Passivation Treatments for ASTM F139 Stainless Steel for Biomedical Applications: Effects on Surface Roughness, Hardening, and Localized Corrosion

Adriana L.Lemos Barboza, Kyung Won Kang, Rita D. Bonetto, Carlos L. Llorente, Pablo D. Bilmes, and Claudio A. Gervasi

(Submitted March 31, 2014; in revised form September 22, 2014; published online November 21, 2014)

Due to the combination of good biofunctionality and biocompatibility at low cost, AISI 316 low carbon vacuum melting (LVM) stainless steel, as considered in ASTM F139 standard, is often the first choice for medical implants, particularly for use in orthopedic surgery. Proper surface finish must be provided to ensure adequate interactions of the alloy with human body tissues that in turn allows the material to deliver the desired performance. Preliminary studies performed in our laboratory on AISI 316LVM stainless steel surfaces modified by glass bead blasting (from industrial supplier) followed by different nitric acid passivation conditions disclosed the necessity to extend parameters of the surface treatments and to further consider roughness, pitting corrosion resistance, and surface and subsurface hardening measurements, all in one, as the most effective characterization strategy. This was the approach adopted in the present work. Roughness assessment was performed by means of amplitude parameters, functional parameters, and an estimator of the fractal dimension that characterizes surface topography. We clearly demonstrate that the blasting treatment should be carried out under controlled conditions in order to obtain similar surface and subsurface properties. Otherwise, a variation in one of the parameters could modify the surface properties, exerting a profound impact on its application as biomaterial. A passivation step is necessary to offset the detrimental effect of blasting on pitting corrosion resistance.

Keywords 316 LVM stainless steel, corrosion, glass bead blasting, hardness, nitric acid passivation, roughness parameters

1. Introduction

Much effort goes into the design, synthesis, and fabrication of biomaterials used in orthopedic surgery that is focused on desired properties governed by bulk structures of the materials (Ref 1). However, appropriate biofunctional behavior depends critically on suitable interactions between the biologic medium and the surface films of an implant material. Consequently, applications of different procedures that modify the original surface are required, for example to improve wear and corrosion resistances. Clearly, obtaining the best performance from these biomaterials presupposes a previous systematic characterization of the effects of surface treatments on chemical composition, micro- or nano-structure, roughness, surface film thickness, and also a correlation of this information with physicochemical properties, biocompatibility, corrosion resistance, etc.

Even though bead blasting, as part of a surface treatment, has been widely studied and applied in connection with Ti c.p. and Ti6Al4V implants (Ref 2-5), only few studies that consider the application of bead blasting on stainless steels as biomaterials are available (Ref 6-9).

Several surface and subsurface modifications result from glass bead blasting (Ref 10). While some of these modifications could be of a chemical nature (Ref 4), others are related to microstructural features, like grain refinement (Ref 6, 7, 11) or are associated with mechanical properties, like hardness or compressive residual stresses (Ref 6, 7, 11-14). In particular, in Ref 9, a discussion can be found on how blasting treatment enhances the surface and subsurface hardness. However, it has been established in the literature (Ref 12) that the increase in surface roughness is the key factor that governs the detrimental effect of blasting on certain forms of corrosion rather than the formation of martensite phase and the generation of the residual stress. Regarding the increase in surface roughness, the

Adriana L. Lemos Barboza, Kyung Won Kang, and **Pablo D. Bilmes,** Laboratorio de Investigaciones de Metalurgia Física (LIMF), Facultad de Ingeniería UNLP, Calle 1 y 47, CP 1900 La Plata, Argentina; **Rita D. Bonetto**, Consejo Nacional de Investigaciones Científicas y Técnicas (CONICET), Facultad de Ciencias Exactas UNLP, Centro de Investigaćn y Desarrollo en Ciencias Aplicadas "Dr. Jorge J. Ronco" (CINDECA), La Plata 1900, Argentina; **Carlos L. Llorente**, Laboratorio de Investigaciones de Metalurgia Física (LIMF), Facultad de Ingeniería UNLP, Calle 1 y 47, CP 1900 La Plata, Argentina and Comisión de Investigaciones Científicas de la Provincia de Buenos Aires (CICPBA), La Plata, Buenos Aires, Argentina; and **Claudio A. Gervasi**, Laboratorio de Investigaciones de Metalurgia Física (LIMF), Facultad de Ingeniería UNLP, Calle 1 y 47, CP 1900 La Plata, Argentina, Consejo Nacional de Investigaciones Científicas y Técnicas (CONICET), Facultad de Ciencias Exactas UNLP, Instituto de Investigaciones Fisicoquímicas Teóricas y Aplicadas (INIFTA), La Plata 1900, Argentina, and Comisión de Investigaciones Científicas de la Provincia de Buenos Aires (CICPBA), La Plata, Buenos Aires, Argentina. Contact emails: adriana.barboza@ing.unlp.edu.ar, adriana.kang@ing.unlp.edu.ar, bonetto@quimica.unlp.edu.ar, cllorent@ing.unlp.edu.ar, pabilmes@ing.unlp.edu.ar, and gervasi@inifta.unlp.edu.ar.

following blasting parameters allow to control the extent of this effect: glass bead size, particle shape and chemical composition, pressure and blasting time (Ref 10). Blasting, the first step of the entire surface treatment, is followed by either chemical passivation or electropolishing as the final step, applied on the blasted surface. This final step aims at achieving effective cleanness and increased corrosion resistance (Ref 15).

The final surface topography obtained on the modified biomaterial governs the interaction with tissues (Ref 16), the degree of corrosive attack by biological fluids (Ref 1), and eventually implant integrity loss. Moreover, release of nonbiocompatible metallic ions during corrosion processes is usually responsible for the occurrence of adverse reactions to the host organism, like hypersensitivity, inflammation, or cytotoxicity (Ref 1, 17).

Recently, preliminary results obtained in our laboratory regarding surface roughness parameters of AISI 316 LVM stainless steel grit blasted for different times and passivated with nitric acid were correlated with localized corrosion resistance measurements (Ref 18). These results clearly showed that it was necessary to extend the ranges for parameters related to the surface treatments and to further consider roughness, pitting corrosion resistance, and surface and subsurface hardening measurements, all in one, as the most effective characterization strategy. This was the approach adopted here to study AISI 316 LVM stainless steel samples with different surface preparations based on blasting with silica particles.

2. Materials and Methods

Cold-rolled AISI 316 LVM stainless steel plates (0.019%C, 1.86%Mn, 17.29%Cr, 2.77%Mo, 14.34%Ni, 0.36%Si, 0.017%P, 0.001%S, 0.14%Cu, 0.086%N) were bead blasted by an industrial supplier for 30 s, 2, 5, and 15 min with silica particles ranging from 30 to 160 μm in diameter at 5 kg/cm^2 pressure without any annealing treatment after bead blasting. These samples were then chemically passivated in 20% HNO_3 (v/v) for 30 and 60 min and in 40% HNO_3 (v/v) for 30 min at room temperature. Results were compared with those samples subjected to mechanical polishing with 6 μm diamond paste with and without 20% HNO_3 (v/v) for 60 min passivation treatment and with blasted samples for 2 min without chemical passivation. Table 1 shows the sample nomenclature used for different treatments. Symbol (I) indicates that the material was sent to the industrial supplier to carry out the blasting treatment for the run-times shown in Table 1. Symbol (II) indicates that the same material was sent in another period of time to the same industrial supplier to carry out the same treatment for the run-times indicated in Table 1.

Measuring surface roughness and topography using 3D SEM observations based on the stereo-pair technique is already an established methodology (Ref 19). The successful use of a commercial software called MeX dates back to nearly 10 years ago (Ref 20). Moreover, an in-depth discussion about uncertainty in topographical measurements using 3D SEM is available from the literature (Ref 21), while a comparison of different surface roughness analysis methods showed that SEM with stereo-pair technique yields the best data resolution (Ref 22). Consequently, this powerful methodology was adopted for use in the present study. Roughness analysis was performed using a scanning electron microscope (SEM) Philips SEM 505 equipped with a digital scanning interface ADA II and a Scandium SIS Image Analysis Software. The working voltage was 25 kV and the spot size was 200 nm. Fifteen stereo pairs of SEM images were obtained at 203× magnification on each blasted and passivated sample and were processed to obtain roughness parameters with EZEImage Program (Ref 19).

The mechanical behavior of different specimen surfaces (bead blasted and as-received specimens subjected to mechanical polishing with 6 μm diamond paste) was evaluated using a microhardness Tester Future Tech FM-700. Vickers microhardness tests were performed on the surfaces and cross sections of specimens with a 10 g force for 10 s (time of loading), according to ASTM E 384-99 (Ref 23).

Electrochemical experiments were performed in deaerated Ringer's solution at 37 ± 1 °C. All potentials were referred to the saturated calomel electrode (SCE). Cyclic potentiodynamic (CP) polarization curves were recorded at a scan rate of 13.8 mV/s between −1.2 and 1.6 V for assessing pitting potential values (E_p). Pitting potentials were considered as the potential at which the current density rose from the passive current density level to reach 200 $\mu A/cm^2$ (Ref 24, 25). We replicated the experiments four times resulting in highly reproducible results. A description of the electrochemical experimental protocol is given in more detail elsewhere (Ref 18).

3. Results and Discussion

3.1 Surface Characterization

The characterization of a surface topography made through roughness parameters is of prime importance in many engineering industries because of its considerable influence on the functional surface properties. There is a great variety and different kinds of parameters depending on what surface characteristics they are describing (amplitude, spatial, hybrid, functional parameters), which can be used to describe surfaces. Deciding which parameter is the most relevant to describe a surface topography with regard to a specific application remains a difficult task (Ref 26-28). Since many of these parameters are not fully reliable to use and interpret, for this work, we selected those with the highest level of acceptance in the field (Ref 3, 29-32). Table 2 shows parameters included in EZEImage program and their meaning. All parameters, except for Sigma, were calculated using the coordinates of the actual measured surface regarding the least squares mean plane.

In the present work, we studied the behavior of amplitude parameters Sq, Sa, Sz, Sku, and Ssk, which provide surface geometric information and functional parameters Sbi, Sci, and Svi. Sa and Sq describe statistical surface height characteristics and they are useful for detecting variations in overall surface height. Sa (Ra in the one-dimensional case) was included because it is widely used for describing surface roughness with blasting treatments (Ref 2-4, 6, 7, 12, 13, 33-35). However, it is important to emphasize that the use of this parameter alone does not always allow thorough surface roughness quantification. Sq represents the profile standard deviation and it is used in skewness and kurtosis computations. According to Dong et al. (Ref 27), Sa parameter does not provide any further information than Sq for many kinds of surfaces, however, Sq has a more significant statistical meaning and therefore these authors suggest using Sq instead of Sa. Nevertheless, we compared both parameters in order to know if their tendency is similar for the surface treatment analyzed here.

Amplitude parameters show the general description of surface topography, and it is important to combine them with

Table 1 Sample nomenclature used for the different surface treatments

Sample nomenclature	Surface treatment
MP	Mechanical polishing with 6 μm diamond paste
MPP2060	Mechanical polishing with 6 μm diamond paste and chemical passivated in 20% HNO_3 (v/v) for 60 min
B30s (I)	Bead blasted for 30 s
B2m (I) and (II)	Bead blasted for 2 min
B5m (I)	Bead blasted for 5 min
B1 m (II)	Bead blasted for 15 min
BP30s2060 (I)	Bead blasted for 30 s and chemical passivated in 20% HNO_3 (v/v) for 60 min
BP2m2060 (I) and (II)	Bead blasted for 2 min and chemical passivated in 20% HNO_3 (v/v) for 60 min
BP5m2060 (I)	Bead blasted for 5 min and chemical passivated in 20% HNO_3 (v/v) for 60 min
BP15m2060 (II)	Bead blasted for 15 min and chemical passivated in 20% HNO_3 (v/v) for 60 min
BP2m2030 (II)	Bead blasted for 2 min and chemical passivated in 20% HNO_3 (v/v) for 30 min
BP2m4030 (II)	Bead blasted for 2 min and chemical passivated in 40% HNO_3 (v/v) for 30 min

Symbols (I) and (II) refer to different sample preparation stages

Table 2 Commonly used parameters on roughness measurements

Parameter	Description
Sigma	Root-mean-square deviation of surface topography (measured regarding the plane which contain the tilt axis)
Sq	Root-mean-square deviation of surface topography (measured regarding the least squares mean plane)
Sa (Ra in 1-D)	Arithmetic mean deviation of surface topography (regarding the least squares mean plane). It is the average surface roughness
Ssk	Skewness of topography height distribution. It is the measure of asymmetry of surface deviations about the mean plane
Sku	Kurtosis of topography height distribution. It is the measure of the peakedness or sharpness of the topography height distribution
Sz	Ten-point height of surface topography. It is defined as the average value of the heights of five highest summits and the depths of five deepest valley points within a sampling area
Sbi	Surface Bearing Index is the ratio of the root-mean-square deviation over the surface height at 5% bearing area. Larger values indicate a large relative bearing area and thus a good bearing property
Sci	Core Fluid Retention Index is the ratio of the void volume of the unit sampling area at the core zone (5-80% bearing area) over the root-mean-square deviation. A larger Sci indicates a good fluid retention in the core zone
Svi	Valley Fluid Retention Index is the ratio of the void volume of the unit sampling area at the valley zone (80-100%) over the root-mean-square deviation. A larger Svi indicates a good fluid retention in the valley zone
D	Estimator of the fractal dimension

functional parameters, such as Sbi, Sci and Svi, which describe important characteristics for many specific applications. These parameters are indexes and they help us understand their meaning since a high or low value of an index is easier to realize in manufacturing processes than the absolute physical quantities. Thus, the index parameters can be used to qualitatively identify the shape features and discriminate in favor of a specific type of three-dimensional surface topography (Ref 27).

Moreover, several works recommend the use of the fractal dimension within the roughness parameters set (Ref 28, 36-39). For example, according to Risović et al. (Ref 38), it can be seen that surfaces with different topographies having the same Ra (Sa in the present study) value have different fractal dimension values. Fractal dimension describes surface irregularity or complexity that cannot be described by roughness parameters used for surface quantitative characterization.

The EZEImage program also provides the necessary data to obtain a fractal dimension estimator D through two different methods. In this paper, the variogram method is used (Ref 40).

The different surface topographies obtained in stages (I) and (II) for the same blasting time and passivation treatment are shown in the SEM images (Fig. 1a and c) and in the surface

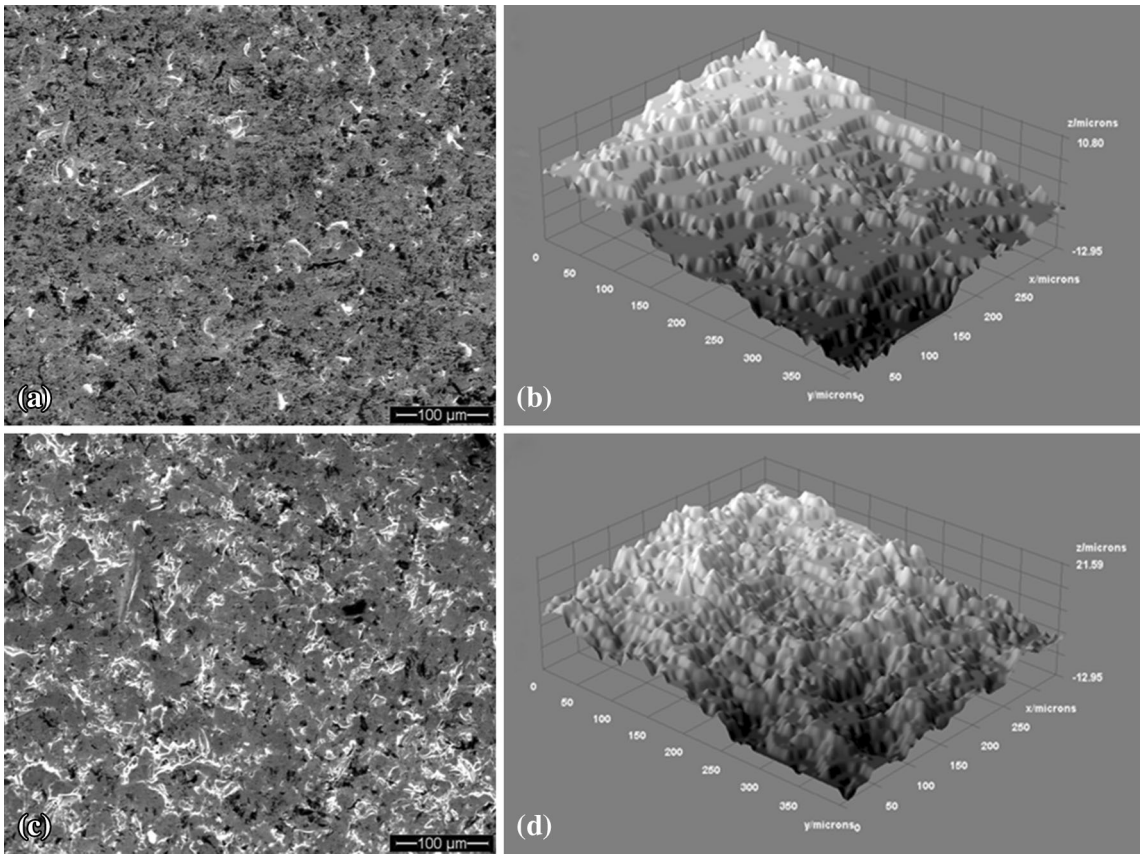

Fig. 1 SEM images and surface plots: (a, b) BP2m2060(I) and (c, d) BP2m2060(II), respectively

plot obtained with the ImageJ software (Ref 41) (Fig. 1b and d). Also, in Fig. 2, it can be observed that the treatment performed in stages (I) and (II) does not generate the same surface characteristics. Figure 2(a) shows that the roughness is greater in stage (II) samples than those made in stage (I), for the same blasting time and chemical passivation but it does not indicate the topographical distribution of the surfaces. With the fractal dimension estimator D (Fig. 2b), it was possible to corroborate that the surfaces do not have the same irregularities.

Although roughness of samples made in stage (II) was larger compared with samples made in stage (I), D showed that the former batch of samples had a more regular surface. These results allow to conclude that parameters used in the blasting process, as the incidence angle, shape and size of particles, etc., were different in both stages (Ref 8, 11, 13, 37).

In Fig. 3, the effect on topography of different chemical passivation treatments in the B2m(II) blasting condition was analyzed. Compared with the sample without passivation only samples with chemical passivation treatments 2030 and 2060 exhibit increased surface roughness (Fig. 3a). Figure 3(b) shows the relationship between Ssk and Svi for these surface conditions. It is observed that the obtained surfaces in the passivated samples BP2m2030(II) or BP2m2060(II) showed fewer valleys (Ssk) and less fluid retention (Svi) than samples B2m(II) and BP2m4030(II). These results can be understood considering that the passivation treatment with 20% HNO_3 attacks the valleys. This attack eliminates irregularities such as ridges inside the valleys and makes them deeper. The final result is an increase in Sa and Sq (Fig. 3a). Also, the bearing curve was re-set when the surface was modified, and therefore the volume ratio considered as valley changed. This change brings about a decrease in Svi and an increase in Sci (Table 3). For sample BP2m2060(II), Ssk decreased and Svi increased with respect to sample BP2m2030(II). This is due to the fact that valleys continued being attacked during the passivation step, making them deeper (Sa and Sq increase) but Ssk becomes reduced to a negligible value compared to that of sample BP2m2030(II). This means that the relative proportion of peaks and valleys became comparable.

On the other hand, it was observed that in stage (I), the application of chemical passivation treatment 2060 did not generate the same intensity of changes on the surface as in stage (II). This was verified by comparison of parameters Sa, Sq, Ssk, and Svi between the conditions B2m(I) and BP2m2060(I) (Table 3; Fig. 2a). As a result, it was observed that surfaces resulting from blasting could vary in their reactivity toward nitric acid attack. Chemical passivation results unable to generate similar final surfaces when it is applied on surfaces that are initially markedly different.

Figures 4(a) and (b) show roughness parameters as a function of the blasting time. Values were normalized to the 30 s value for stage (I) and to the 2 min value for stage (II). In stage (I), high- and low-extreme roughness parameter values were observed at 2 min. The increase in San and Sqn after 30 s of blasting indicates that the surface height difference increases while the decrease in Skun shows that the peak distribution is more Gaussian. Changes resulting after 5 min of blasting were not so marked, although a decrease in San and Sqn values was

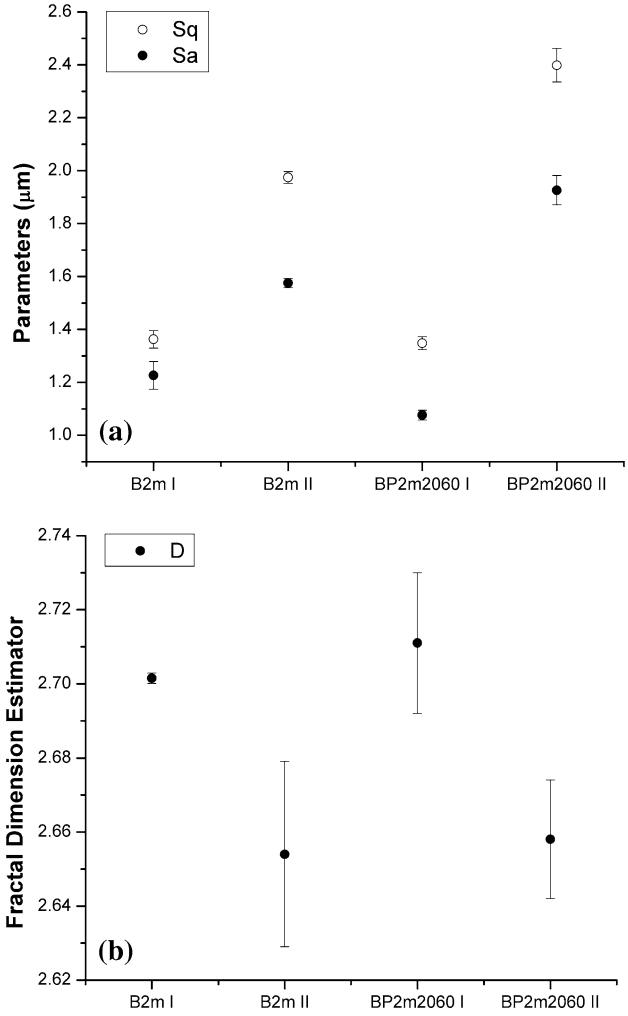

Fig. 2 (a) Sq and Sa parameters and (b) Fractal dimension estimator D for B2 min (I) and (II) and, BP2m2060 (I) and (II)

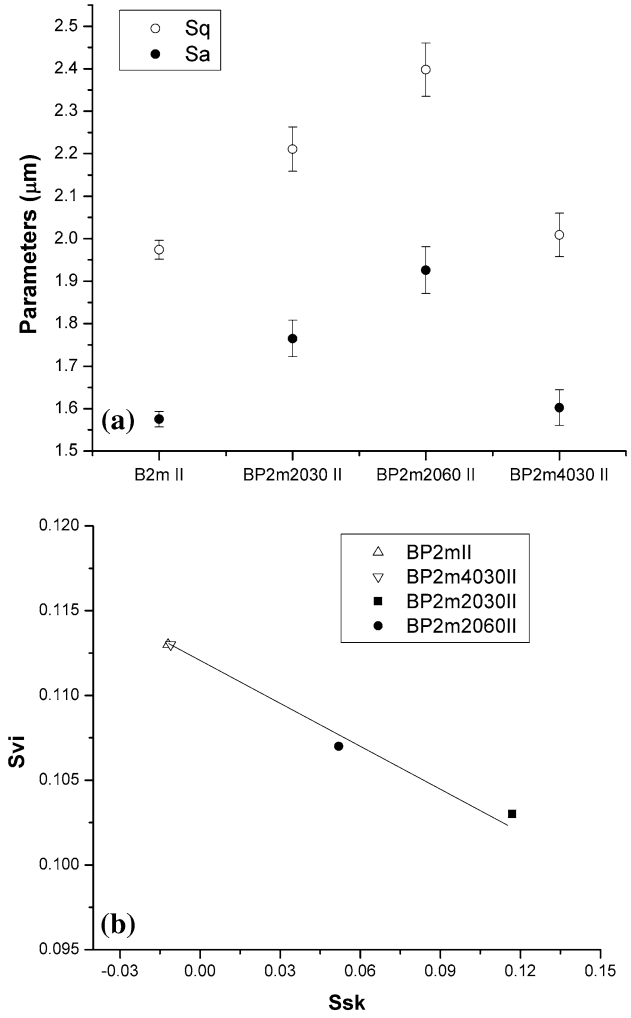

Fig. 3 Effect of nitric acid passivation on 2 min blasted samples [stage (II)] on (a) Sq and Sa parameters; (b) relationship between Svi and Ssk

measured as well as a slight increase in Skun. This behavior, also observed for stage (II) in the blasting time window of 2 to 15 min, is due to a phenomenon known as over blasting (Ref 11, 14). After some time of blasting, the surface layer was work-hardened and no significant increase in roughness by plastic deformation was possible. In addition, peaks on the surface started to flatten. This effect can be observed through variations in parameter Sz in both stages (I and II). Thus, Sz values decreased with increasing blasting time.

Regarding functional parameters, it can be observed that in stage (I) parameters Sbin and Scin are highly sensitive to the different surface characteristics of the samples, while in stage (II) Svin and Scin parameters are the most sensitive. Arvidsson et al. Ref 3 found that the most sensitive parameters for blasted surfaces were Sbi and Sci, although they proposed that only Sci should be taken into account for surface characterization. In this work, Sci varies simultaneously with either Sbi or Svi and consequently, the analysis of two combined parameters, i.e., Sci-Sbi or Sci-Svi, provides more information. In short, it is meaningful to study all parameters that are modified, either of amplitude or functional, since this enables a better qualitative description of the changes that undergo peaks, valleys, and cores according to the different topographies. For instance, regarding the analysis of the chemical passivation effect in stage (II), the variation of parameters Svi and Sci took place with a variation of parameters Ssk and Sa or Ssk and Sq.

According to the presented results, Sa and Sq variations were so similar that it was enough to use only one of them in connection with changes in roughness resulting from a blasting step. Nevertheless, in order to analyze changes in the topography, it is necessary, in some cases, to combine Sa or Sq with other parameters like fractal dimension estimator D and functional parameters, as was shown in this work.

3.2 Microhardness Measurements

Examination of cross sections of samples B30s(I) and B2m(I) by SEM (Fig. 5) revealed the presence of an irregular morphology deformed at the subsurface. This deformed zone increased in thickness for blasting times longer than 30 s. SEM micrographs of the other samples at different blasting times showed the same morphology as B2m(I). Blasting process generates a strong plastic deformation at the surface, which affects microstructure and mechanical properties of the material

Table 3 Some amplitude and functional parameters values obtained with scanning electron microscope (SEM)

Parameter	B2m (I)	BP2m2060 (I)	B2m (II)	B2m2030 (II)	B2m2060 (II)	B2m4030 (II)
Ssk	0.074 ± 0.047	0.043 ± 0.032	−0.012 ± 0.041	0.117 ± 0.038	0.052 ± 0.045	−0.011 ± 0.046
Sz (μm)	15.360 ± 1.225	14.254 ± 0.851	17.301 ± 0.773	20.032 ± 0.856	22.524 ± 0.793	17.330 ± 0.662
Sci	1.584 ± 0.023	1.575 ± 0.015	1.561 ± 0.016	1.612 ± 0.018	1.585 ± 0.017	1.576 ± 0.013
Svi	0.108 ± 0.003	0.111 ± 0.003	0.113 ± 0.002	0.103 ± 0.003	0.107 ± 0.003	0.113 ± 0.002

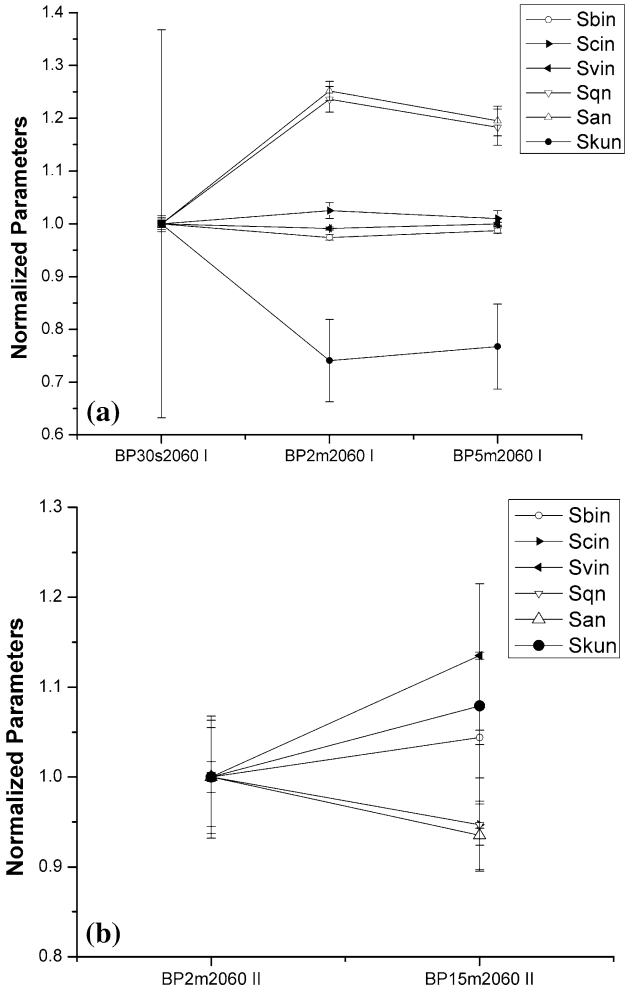

Fig. 4 (a) RP values normalized to 30 s value as a function of blasting time with the same passivation treatment for samples made in stage (I); (b) idem (a) but made in stage (II) and normalized to 2 min value

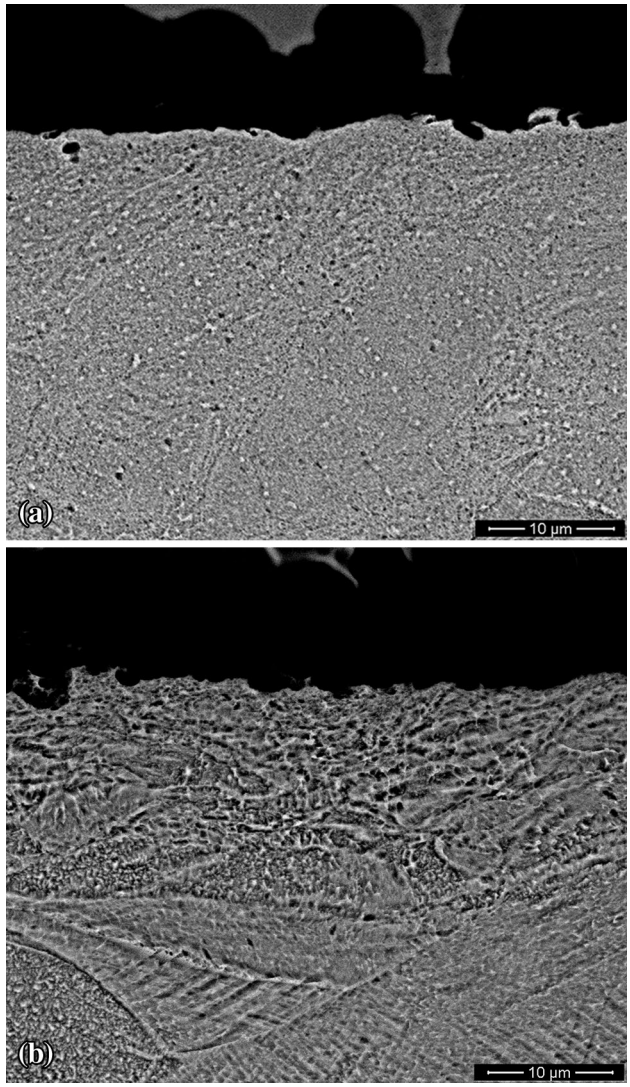

Fig. 5 Cross-section SEM images of samples (a) B30 s(I) and (b) B2 m(I)

surface and subsurface. As the surface deformation is increased, crystalline defects are increased (dislocations, twinning, etc.). The existence of a high density of dislocations makes their movements difficult and produces an increase in the material hardness (Ref 7, 42, 43).

Surface microhardness values for different blasting times and process stages are shown in Table 4 together with the value for MP condition. Surface hardness increased with bead blasting time within each stage and was always larger than that measured for MP. Surface hardness is smaller for sample B2m(II) as compared with sample B2m(I). This could result from the use of different process parameters, like for example the blasting angle (Ref 11, 13). Also, if the process parameters had been the same in the two stages, the surface hardness of B15m(II) should have been larger than B5m(I) (Ref 14).

Figure 6 shows a cross-section hardness distribution of the blasted samples measured along a line perpendicular to the surface. Hardness measurements gradually decreased with increasing distance from the surface for all different bead blasting times and stages. The depth penetration of the hardened layer ranged between 40 and 60 μm depending on the blasting condition.

Figure 6(a) shows that in sample B2m(I) the hardened layer extends to a greater depth than in samples B30s(I) and B5m(I).

Table 4 Surface microhardness values and standard deviations for different blasting times and process stages and for MP conditions

	MP	B30s (I)	B2m (I)	B5m (I)	B2m (II)	B15m (II)
Hardness (HV)	301 ± 12	461 ± 10	500 ± 11	539 ± 12	447 ± 11	530 ± 11

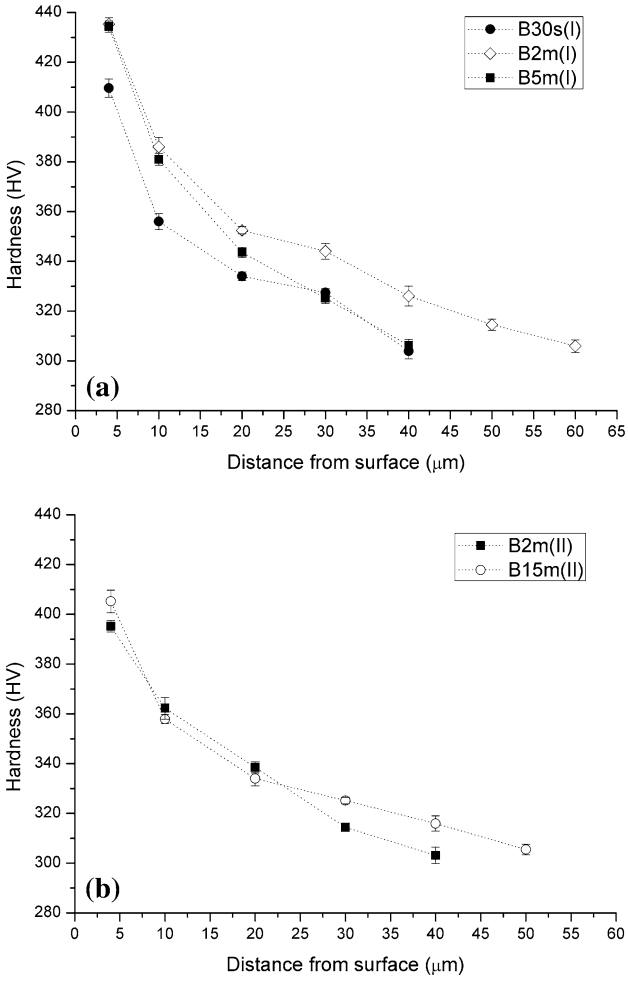

Fig. 6 Microhardness profile of (a) 30 s, 2 min, and 5 min blasting times for samples made in stage (I) and (b) 2 min and 15 min blasting times for samples made in stage (II)

However, B5m(I) should have exhibited the greatest depth of penetration or at least the same as B2m(I) if the process parameters had been the same in both blasting treatments. Noteworthy, it was shown that if the incidence angle is varied, the depth of hardness penetration would also vary without changing the other blasting parameters (Ref 11).

Moreover, samples B2m(I) and B5m(I) show similar hardness values near the surface. On the other hand, for samples made in stage (II), hardness decreased gradually with the distance from the surface and with bead blasting time, as shown in Fig. 6(b).

Figure 7 compares cross-section hardness distribution of samples blasted for 2 min in the two stages, i.e., B2m(I) and B2m(II). B2m(I) had larger hardness near the surface and greater depth of penetration than B2m(II). Hardness and

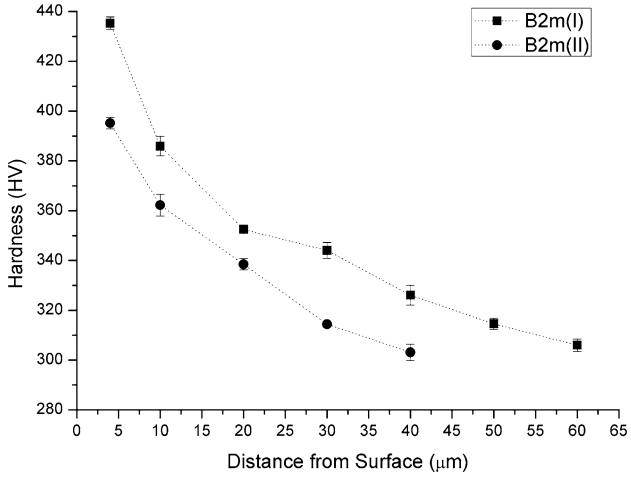

Fig. 7 Microhardness profile of 2 min blasting time for samples made in stage (I) and (II)

penetration depth should be equal from one stage to another if the operating parameters had been the same. This, added to the fact that B5m(I) did not show the expected trend, i.e., equal or greater depth of penetration hardness than B2m(I), suggests that the process parameters not only changed from one stage to another but also from one condition to another within the same stage.

3.3 Electrochemical Characterization

CP polarization curves in Fig. 8 show, during the anodic scan, corrosion potentials of approximately −1.0 V followed by a passivity region and finally the initiation and propagation of pitting corrosion at potentials more anodic than E_p. For the sake of clarity, hysteresis loops obtained during the cathodic scans are not shown in Fig. 8. Polarization curves for MP and MPP2060 conditions can be seen in the inset in Fig. 8 and confirm the beneficial effect of the passivation step. Thus, for the surface condition MPP2060, a current peak can be observed in the CP polarization curve which initiates at around 0.6 V. This current peak corresponds to the transpassive oxidation of Cr(III) species in the oxide to Cr(IV) species and E_p cannot be detected what points to the fact that under the selected experimental variables (electrolyte composition and temperature), this surface condition has an excellent pitting resistance. In this work, we focused our corrosion-related analysis (as is typical for all stainless steels) to localized corrosion that could take place in the event of an increase in the oxidizing power of the environment. Clearly, corrosion processes for these alloys occurring at a corrosion potential that lies within the passive region (Fig. 8) are not expected to be of main concern. Transpassive behavior can only be detected in connection with sample MPP2060 because for the rest of the studied conditions pitting corrosion starts at more active potentials during the

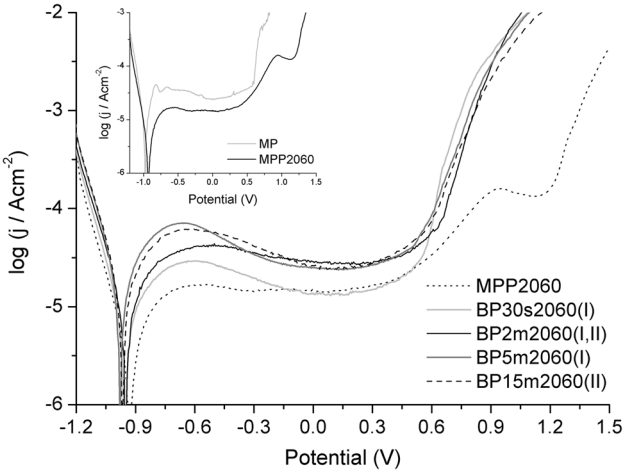

Fig. 8 Polarization curves of samples chemically passivated and blasted for different times as well as samples mechanically polished and chemically passivated. Inset graph shows polarization curves of MPP2060 and MP samples (see Table 1 for sample nomenclature)

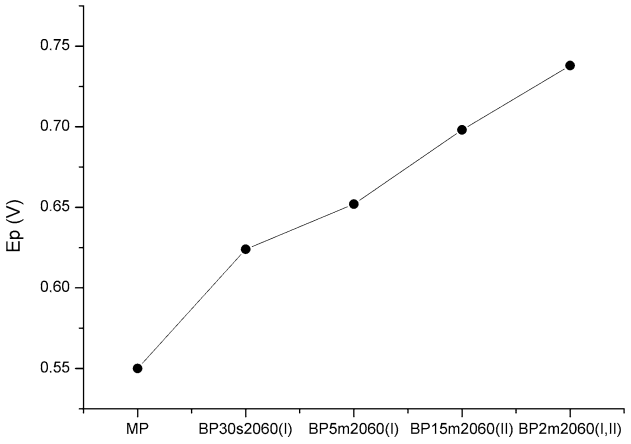

Fig. 9 Pitting potentials E_p for samples chemically passivated and blasted for different times as well as samples mechanically polishing (see Table 1 for the definitions of the abbreviations in *x*-axis)

anodic scan. In other words, local breakdown of the passive layer takes place at pit initiation sites at less anodic potentials than the potential window for the transpassive oxidation, and the current rises rapidly due to the anodic dissolution of the alloy inside the pits.

Figure 9 shows pitting potential values measured for the different surface treatments as indicated in the *x*-axis of the plot. E_p values for blasted and passivated samples in stage (I) shown in Fig. 9 decrease according to the following sequence BP2m2060(I) > BP5m2060(I) > BP30s2060(I). BP2m2060(I) condition was compared to BP2m2060(II) condition since the blasting treatment was performed in two different stages. There is no significant difference between the pitting potentials measured for each of the two conditions and consequently both will be renamed BP2m2060(I,II) in the text below.

Condition BP15m2060(II) shows a pitting potential lower than BP2m2060(I,II) but higher than B5m2060(I) (Fig. 9). This means that 2 min is the optimal blasting time for avoiding lower pitting corrosion resistances in the studied system.

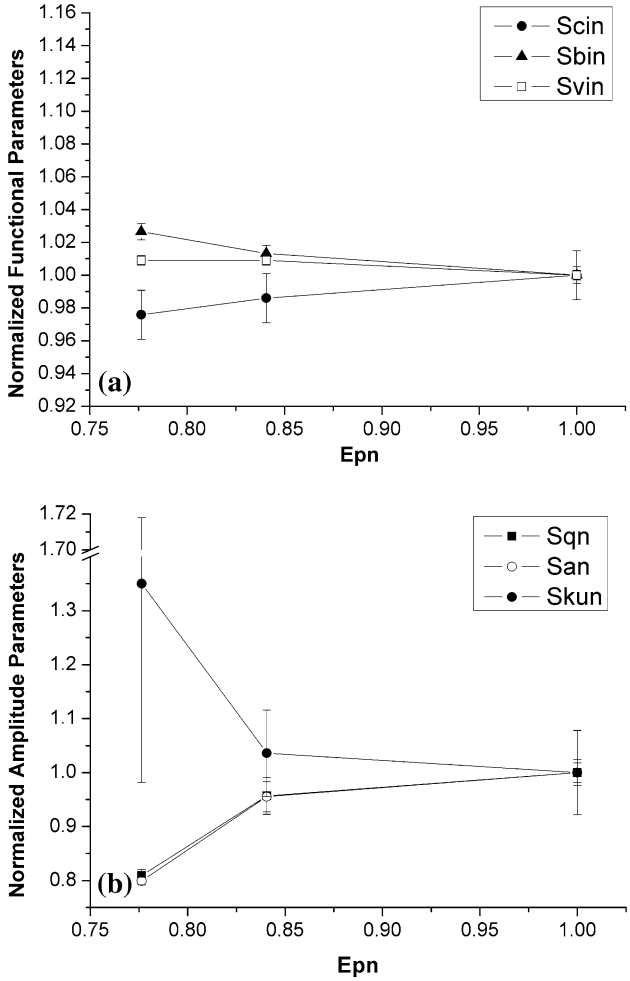

Fig. 10 E_p and roughness parameters values normalized to 2 min value for samples obtained in stage (I) (a) functional parameters as a function of Epn; (b) amplitude parameters as a function of Epn. All the samples were passivated in 20% HNO_3 for 60 min

Blasting with passivation treatment decreased localized corrosion resistance of AISI 316 LVM in comparison with condition MPP2060. Noteworthy, studies on pitting corrosion in blasted samples (Ref 4, 13, 33) showed that the effect of blasting without subsequent passivation is a shift of E_p values in the less noble direction.

3.4 Discussion

As we pointed out throughout this work, blasting increases the implant roughness and also increases the surface and subsurface hardness. Since this process of surface modification cannot produce a fully passivated and impurity-free surface, according to standard ASTM 86-12, it is essential that the surface treatment includes a chemical passivation step to increase the corrosion resistance of the implant. Such a surface treatment results in the surface properties required in implants, namely, high corrosion and wear resistances and improved biocompatibility. This, in turn, preserves the biomaterial bulk properties and reduces costs significantly.

From the results presented in this work, it can be observed that the blasting process parameters not only changed from one

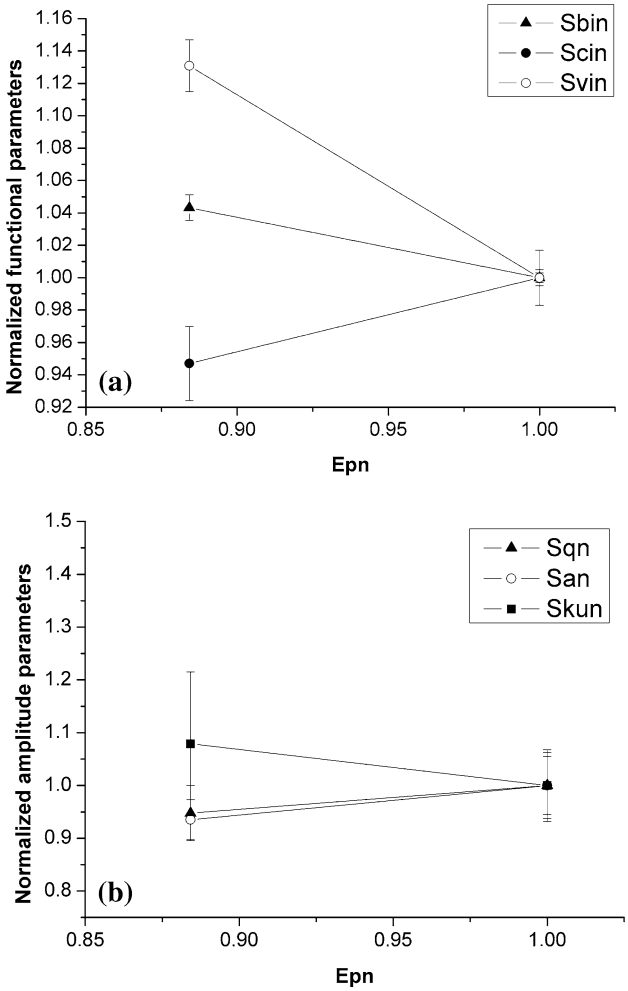

Fig. 11 E_p and roughness parameters values normalized to the 2 min value for samples obtained in stage (II) (a) functional parameters as a function of Epn; (b) amplitude parameters as a function of Epn. All the samples were passivated in 20% HNO_3 for 60 min

stage to another but also from one condition to another within the same stage. This can lead to different topographies and mechanical properties for different manufacturing batches and consequently to modifications in the implant behavior and its interactions with the living tissue. Because of that, it is important to carry out quality monitoring of the manufactured implants through techniques such as roughness measurement, hardness, and localized corrosion testing.

The relationship between Epn (E_p normalized to the 2 min value) and roughness parameter values normalized to the 2 min value for samples made in stage (I) is shown in Fig. 10 and for samples made in stage (II) is shown in Fig. 11, namely as Sqn, San, Skun, Sbin, Svin, and Scin. All the samples were passivated with 20% HNO_3 (v/v) for 60 min.

There are several surface characteristics described with different roughness parameters that can cause an increment in the pitting potential and it was found that these characteristics are related between them. Also, it was observed that the more Gaussian the surface (decrease of Sku toward values close to 3), the higher the value of E_p (Fig. 4 and 9). In turn, the symmetrization of the surface roughness caused an increase in the distance between the peaks and valleys (increase in San and Sqn), and this effect was accompanied by a decrease in the fluid retention capacity in the valley but an increase in the fluid retention capacity in the core. Similarly, as explained in section 3.1, regarding the effect of chemical passivation in the resulting surfaces (Fig. 3), the changes in topography that can decrease the susceptibility to pitting corrosion are related to certain characteristics of the valley and core surfaces. Surface characteristics that induce smaller values of E_p are a higher number of imperfections with narrower core (smaller values of Scin and higher values of Svin). In this case, the electrolyte exchange within the valley will be inhibited and it would favor blockage conditions. Reducing these imperfections and increasing Scin contribute to electrolyte exchange and consequently to enhanced pitting corrosion resistance. These conclusions are similar to those of Faller et al. (Ref 33), although they used roughness profiles and only Ra values.

4. Conclusions

We emphasize the importance of selecting an adequate set of roughness parameters for characterizing surface treatments of biomaterials. This selection enables to correlate design parameters for the treatments with final surfaces and to verify surfaces reproducibility.

Roughness parameters like Sa or Sq (easily measurable with a profilometer) and hardness would provide satisfactory quantitative methods of monitoring on-line blasting process rather than the qualitative operator-based methods currently used. Nevertheless, in order to analyze changes in the topography, it may be necessary to combine Sa or Sq with other parameters like fractal dimension D and functional parameters.

From the point of view of pitting corrosion optimal surface treatment, conditions for ASTM F139 stainless steel for biomedical applications in deaerated Ringer's solution at 37 ± 1 °C correspond to a blasting time of 2 min. Performing a passivation step is particularly important to avoid impairing severely the pitting resistance of the blasted samples. The best results can be obtained through chemical passivation in 20% HNO_3 (v/v) for 60 min.

Acknowledgments

The authors acknowledge the staff of the Microscopy Laboratory of Centro de Investigación y Desarrollo en Ciencias Aplicadas "Dr. Jorge J. Ronco" (CINDECA) for technical support in the acquisition of SEM images.

References

1. B.D. Ratner, and A.S. Hoffman, *Thin Films, Grafts, and Coatings, Biomaterials Science: An Introduction to Materials in Medicine*, 1st ed., B.D. Ratner, A.S. Hoffman, F.J. Schoen, and J.E. Lemons, Eds., Academic Press, 1996, p 105–118
2. C. Aparicio, F.J. Gil, C. Fonseca, M. Barbosa, and J.A. Planell, Corrosion Behaviour of Commercially Pure Titanium Shot Blasted with Different Materials and Sizes of Shot Particles for Dental Implant Applications, *Biomaterials*, 2003, **24**(2), p 263–273
3. A. Arvidsson, B.A. Sater, and A. Wennerberg, The Role of Functional Parameters for Topographical Characterization of Bone-Anchored Implants, *Clin. Implant Dent. Relat Res.*, 2006, **8**(2), p 70–76

4. V. Barranco, M.L. Escudero, and M.C. García-Alonso, 3D, Chemical and Electrochemical Characterization of Blasted Ti6Al4V Surfaces: Its Influence on the Corrosion Behaviour, *Electrochim. Acta*, 2007, **52**(13), p 4374–4384
5. V. Barranco, E. Onofre, M.L. Escudero, and M.C. García-Alonso, Characterization of Roughness and Pitting Corrosion of Surfaces Modified by Blasting and Thermal Oxidation, *Surf. Coat. Technol.*, 2010, **204**(23), p 3783–3793
6. M. Multigner, E. Frutos, J.L. González-Carrasco, J.A. Jiménez, P. Marín, and J. Ibáñez, Influence of the Sandblasting on the Subsurface Microstructure of 316LVM Stainless Steel: Implications on the Magnetic and Mechanical Properties, *Mater. Sci. Eng. C*, 2009, **29**(4), p 1357–1360
7. M. Multigner, S. Ferreira-Barragáns, E. Frutos, M. Jaafar, J. Ibáñez, P. Marín, M.T. Pérez-Prado, G. González-Doncel, A. Asenjo, and J.L. González-Carrasco, Superficial Severe Plastic Deformation of 316 LVM Stainless Steel Through Grit Blasting: Effects on Its Microstructure and Subsurface Mechanical Properties, *Surf. Coat. Technol.*, 2010, **205**(7), p 1830–1837
8. J.C. Galván, L. Saldaña, M. Multigner, A. Calzado-Martín, M. Larrea, C. Serra, N. Vilaboa, and J.L. González-Carrasco, Grit Blasting of Medical Stainless Steel: Implications on its Corrosion Behavior, Ion Release and Biocompatibility, *J. Mater. Sci. Mater. Med.*, 2012, **23**(3), p 657–666
9. B. Arifvianto, S. Wibisono, and M. Mahardika, Influence of Grit Blasting Treatment Using Steel Slag Balls on the Subsurface Microhardness, Surface Characteristics and Chemical Composition of Medical Grade 316L Stainless Steel, *Surf. Coat. Technol.*, 2012, **210**, p 176–182
10. F. Reidenbach, *ASM Metals Handbook Volume 5: Surface Engineering*, 10th ed., ASM International, 1994
11. K. Poorna Chander, M. Vashista, K. Sabiruddin, S. Paul, and P.P. Bandyopadhyay, Effects of Grit Blasting on Surface Properties of Steel Substrates, *Mater. Des.*, 2009, **30**(8), p 2895–2902
12. F. Otsubo, K. Kishitake, T. Akiyama, and T. Terasaki, Characterization of Blasted Austenitic Stainless Steel and Its Corrosion Resistance, *J. Therm. Spray Technol.*, 2003, **12**(4), p 555–559
13. A. BenRhouma, H. Sidhom, C. Braham, J. Lédion, and M.E. Fitzpatrick, Effects of Surface Preparation on Pitting Resistance, Residual Stress, and Stress Corrosion Cracking in Austenitic Stainless Steels, *J. Mater. Eng. Perform.*, 2001, **10**(5), p 507–514
14. A.W. Momber and Y.C. Wong, Overblasting Effects on Surface Properties of Low-Carbon Steel, *J. Coat. Technol. Res.*, 2005, **2**(6), p 453–461
15. L.J. Korb, and D.L. Olson, *ASM Metals Handbook Volume 13: Corrosion*, 9th ed., ASM International, 1987
16. A. Wennerberg and T. Albrektsson, Effects of Titanium Surface Topography on Bone Integration: A Systematic Review, *Clin. Oral Implants Res.*, 2009, **20**(4), p 172–184
17. R. Singh and N.B. Dahotre, Corrosion Degradation and Prevention by Surface Modification of Biometallic Materials, *J. Mater. Sci. Mater. Med.*, 2007, **18**(5), p 725–751
18. M.D. Pereda, K.W. Kang, R. Bonetto, C. Llorente, P. Bilmes, and C. Gervasi, Impact of Surface Treatment on the Corrosion Resistance of ASTM F138-F139 Stainless Steel for Biomedical Applications, *Proc. Mater. Sci.*, 2012, **1**, p 446–453
19. E. Ponz, J.L. Ladaga, and R.D. Bonetto, Measuring Surface Topography with Scanning Electron Microscopy. I. EZEImage: A Program to Obtain 3D Surface Data, *Microsc. Microanal.*, 2006, **12**(2), p 170–177
20. P. Bariani, L. De Chiffre, H.N. Hansen, and A. Horsewell, Investigation on the Traceability of Three Dimensional Scanning Electron Microscope Measurements Based on the Stereo-Pair Technique, *Precis. Eng.*, 2005, **29**, p 219–228
21. K.W. Kang, M.D. Pereda, M.E. Canafoglia, P. Bilmes, C. Llorente, and R. Bonetto, Uncertainty Studies of Topographical Measurements on Steel Surface Corrosion by 3D Scanning Electron Microscopy, *Micron*, 2012, **43**, p 387–395
22. H. Ostadi and K. Jiang, D.W.L. Hukins., A Comparison of Surface Roughness Analysis Methods Applied to Urinary Catheters, *Precis. Eng.*, 2010, **34**, p 798–801
23. ASM, *Standard Test Method for Microindentation Hardness of Materials*", E384-99, ASTM Standards
24. H.C. Man and D.R. Gabe, The Determination of Pitting Potentials, *Corros. Sci.*, 1981, **21**(4), p 323–326
25. M.D. Pereda, C.A. Gervasi, C.L. Llorente, and P.D. Bilmes, Microelectrochemical Corrosion Study of Supermartensitic Welds in Chloride-Containing Media, *Corros. Sci.*, 2011, **53**(12), p 3934–3941
26. K.J. Stout, P.J. Sullivan, W.P. Dong, E. Mainsah, N. Luo, T. Mathia, and H. Zahouani, *The Development of Methods for the Characterization of Roughness in Three Dimensions*, University of Birmingham, Commission of the European Communities, Great Britain, 1993
27. W.P. Dong, P.J. Sullivan, and K.J. Stout, Comprehensive Study of Parameters for Characterising Three- Dimensional Surface Topography: III: Parameters for Characterising Amplitude and Some Functional Properties, *Wear*, 1994, **178**(1–2), p 29–43
28. M. Bigerelle, D. Najjar, T. Mathia, A. Iost, T. Coorevits, and K. Anselme, An Expert System to Characterise the Surfaces Morphological Properties According to their Tribological Functionalities: The Relevance of a Pair of Roughness Parameters, *Tribol. Int.*, 2013, **59**, p 190–202
29. L.T. Brown, "The Use of 3D Surface Analysis Techniques to Investigate the Wear of Matt Surface Finish Femoral Stems in Total Hip Replacement", Ph.D. Thesis, University of Huddersfield, 2006
30. C. Cionea, "Microstructural Evolution of Surface Layers during Electrolytic Plasma Processing", Ph.D. Thesis, University of Texas at Arlington, 2010
31. M. Niemczewska-Wojcik, The Influence of the Surface Geometric Structure on the Functionality of Implants, *Wear*, 2011, **271**(3–4), p 596–603
32. J. Löberg, "Integrated Biomechanical, Electronic and Topographic Characterization of Titanium Dental Implants", Ph.D. Thesis, University of Gothenburg, 2011
33. M. Faller, S. Buzzi, and O. Trzebiatowski, Corrosion Behaviour of Glass-Bead Blasted Stainless Steel Sheets and Other Sheets with Dull Surface Finish in a Chloride Solution, *Mater. Corros.*, 2005, **56**(6), p 373–378
34. P. O'Hare, B.J. Meenan, G.A. Burke, G. Byrne, D. Dowling, and J.A. Hunt, Biological Responses to Hydroxyapatite Surfaces Deposited Via a Co-Incident Microblasting Technique, *Biomaterials*, 2010, **31**(3), p 515–522
35. R.A. Gittens, T. McLachlan, R. Olivares-Navarrete, Y. Cai, S. Berner, R. Tannenbaum, Z. Schwartz, K.H. Sandhage, and B.D. Boyan, The Effects of Combined Micron-/Submicron-Scale Surface Roughness and Nanoscale Features on Cell Proliferation and Differentiation, *Biomaterials*, 2011, **32**(13), p 3395–3403
36. T. Provder and B. Kunz, Application of Profilometry and Fractal Analysis to the Characterization of Coatings Surface Roughness, *Prog. Org. Coat.*, 1996, **27**(1–4), p 219–226
37. S. Amada and T. Hirose, Influence of Grit Blasting Pre-Treatment on the Adhesion Strength of Plasma Sprayed Coatings: Fractal Analysis of Roughness, *Surf. Coat. Technol.*, 1998, **102**(1–2), p 132–137
38. D. Risović, S.M. Poljaček, and M. Gojo, On Correlation Between Fractal Dimension and Profilometric Parameters in Characterization of Surface Topographies, *Appl. Surf. Sci.*, 2009, **255**(7), p 4283–4288
39. X. Liang, B. Lin, X. Han, and S. Chen, Fractal Analysis of Engineering Ceramics Ground Surface, *Appl. Surf. Sci.*, 2012, **258**(17), p 6406–6415
40. R.D. Bonetto, J.L. Ladaga, and E. Ponz, Measuring Surface Topography by Scanning Electron Microscopy. II. Analysis of Three Estimators of Surface Roughness in Second Dimension and Third Dimension, *Microsc. Microanal.*, 2006, **12**(2), p 178–186
41. W.S. Rasband, ImageJ, U.S. National Institutes of Health, Bethesda, MD, USA, 2012. http://rsb.info.nih.gov/ij/index.html
42. V. Azar, B. Hashemi, and M. RezaeeYazdi, The Effect of Shot Peening on Fatigue and Corrosion Behavior of 316L Stainless Steel in Ringer's Solution, *Surf. Coat. Technol.*, 2010, **204**(21–22), p 3546–3551
43. F.J. Gil, J.A. Planell, A. Padrós, and C. Aparicio, The Effect of Shot Blasting and Heat Treatment on the Fatigue Behavior of Titanium for Dental Implant Applications, *Dental Mater.*, 2007, **23**(4), p 486–491